

11. Anderson, M. P. *et al. Science* **251**, 679–682 (1991).
12. Kärner, N. *et al. Cell* **64**, 681–691 (1991).
13. Anderson, M. P. *et al. Science* **253**, 202–205 (1991).
14. Dharmasathaporn, K., McRoberts, J. A., Mandel, K. G., Tisdale, L. D. & Masui, H. *Am. J. Physiol.* **266**, G204–G208 (1994).
15. Schoumacher, R. A. *et al. Proc. natn. Acad. Sci. U.S.A.* **87**, 4012–4016 (1990).
16. Bauer, C. K., Steinmeyer, K., Schwarz, J. R. & Jentsch, T. J. *Proc. natn. Acad. Sci. U.S.A.* **88**, 11052–11056 (1991).
17. Miller, C. & Richard, E. A. in *Chloride Channels and Carriers in Nerve, Muscle, and Glial Cells* (eds Alvarez-Leefmans, F. J. & Russel, J. M.) 383–405 (Plenum, New York 1990).
18. Kreusel, K.-M., Fromm, M., Schulze, J.-D. & Hegel, U. *Am. J. Physiol.* **261**, C574–C582 (1991).
19. Solc, C. K. & Wine, J. J. *Am. J. Physiol.* **261**, C658–C674 (1991).
20. Cliff, W. H. & Frizzell, R. A. *Proc. natn. Acad. Sci. U.S.A.* **87**, 4956–4960 (1990).
21. Anderson, M. P. & Welsh, M. J. *Proc. natn. Acad. Sci. U.S.A.* **88**, 6003–6007 (1991).
22. Worrell, R. T. & Frizzell, R. A. *Am. J. Physiol.* **260**, C877–C882 (1991).
23. Ward, C. L., Krouse, M. E., Gruenert, D. C., Kopito, R. R. & Wine, J. J. *Proc. natn. Acad. Sci. U.S.A.* **88**, 5277–5281 (1991).
24. Tabcharani, J. A., Low, W., Elie, D. & Hanrahan, J. W. *FEBS Lett.* **270**, 157–164 (1990).
25. Hyde, S. C. *et al. Nature* **346**, 362–365 (1990).
26. Drumm, M. L. *et al. Cell* **62**, 1227–1233 (1990).
27. Rich, D. P. *et al. Science* **253**, 205–207 (1991).
28. Tabcharani, J. A., Chang, X.-B., Riordan, J. R. & Hanrahan, J. W. *Nature* **352**, 628–631 (1991).
29. Cheng, S. H. *et al. Cell* **66**, 1027–1036 (1991).
30. Kyte, J. & Doolittle, R. F. *J. molec. Biol.* **157**, 105–132 (1982).
31. Kozak, M. *J. Cell Biol.* **115**, 887–903 (1991).
32. Higuchi, R. in *PCR Technology* (ed. Erlich, H. A.) 61–70 (Stockton, New York, 1989).
33. Colman, A. in *Transcription and Translation* (eds Hames, B. D. & Higgins, S. J.) 271–302 (IRL, Oxford, 1984).

ACKNOWLEDGEMENTS. We thank B. König for technical assistance, K. Steinmeyer for help with northern blots and for discussion, and S. Morley and W. Meyerhof for the rat brain cDNA library. This work was supported, in part, by the BMFT, the US Cystic Fibrosis Foundation, and the Deutsche Forschungsgemeinschaft.

## Delay in vesicle fusion revealed by electrochemical monitoring of single secretory events in adrenal chromaffin cells

Robert H. Chow, Ludolf von Rüden & Erwin Neher\*

Max-Planck-Institut für biophysikalische Chemie, Postfach 2841, Am Fassberg, D-3400 Göttingen, Germany

**IN synapses, a rise in presynaptic intracellular calcium leads to secretory vesicle fusion in less than a millisecond, as indicated by the short delay from excitation to postsynaptic signal<sup>1–4</sup>. In non-synaptic secretory cells, studies at high time resolution have been limited by the lack of a detector as fast and sensitive as the postsynaptic membrane. Electrochemical methods may be sensitive enough to detect catecholamines released from single vesicles<sup>5,6</sup>. Here, we show that under voltage-clamp conditions, stochastically occurring signals can be recorded from adrenal chromaffin cells using a carbon-fibre electrode as an electrochemical detector. These signals obey statistics characteristic for quantal release; however, in contrast to neuronal transmitter release, secretion occurs with a significant delay after short step depolarizations. Furthermore, we identify a pedestal or 'foot' at the onset of unitary events which may represent the slow leak of catecholamine molecules out of a narrow 'fusion pore' before the pore dilates for complete exocytosis.**

Isolated bovine chromaffin cells were used to study catecholamine release under patch-clamp whole-cell recording conditions. We applied short step depolarizations to open voltage-gated calcium channels<sup>7</sup>, thereby injecting calcium to activate secretion<sup>8</sup>. When the tip of a carbon-fibre electrode<sup>9,10</sup> was placed less than 1 µm from the cell to record in amperometric mode, spike-like current transients were seen at variable times after the onset of depolarizing pulses (see Fig. 1a). These signals occurred rarely or not at all, unless the cell had been stimulated; on stimulation they appeared with a frequency that peaked shortly after the voltage step and that subsequently decayed over about 100 ms. Furthermore, they were seen only if the potential applied to the carbon-fibre electrode was greater than about 250 mV (exceeding the oxida-

TABLE 1 Single secretory events follow a Poisson distribution

Cells	$n_0$	$n_1$	$n_2$	$n_3$	$n_{\geq 3}$	$N$	events
<b>A</b>							
Observed	45	52	26	7	3	133	139
Calc. ( $m=1.01$ )	47	49	26	9	2		
<b>B</b>							
Observed	8	18	17	12	10	65	133
Calc. ( $m=2.05$ )	8	17	18	12	10		
<b>C</b>							
Observed	15	28	20	8	3	74	105
Calc. ( $m=1.42$ )	18	25	18	9	4		
<b>D</b>							
Observed	28	19	11	0	0	58	41
Calc. ( $m=0.71$ )	29	20	7	2	0		

Three cells with a low probability of release were selected for analysis. Cells A, B, C and D were repetitively stimulated every 5 s by depolarizing pulses to +10 mV for 25 ms (A, C) or 50 ms (B, D). D was, in fact, the same cell as C, but at a much later time in the experiment, when the release probability had decreased. Each discernible current transient, regardless of size, was counted as one event.  $n_{0,1,2,3,\dots,x}$ : numbers of times that pulses elicited 0, 1, 2, 3, ..., x events during the 5-s interval after a pulse. Calculated numbers: from Poisson's law

$$P_x = n_x/N = e^{-m} m^x / x!$$

$N$ , Total number of step depolarizations.

$m$ , (total number of events)/ $N = (n_1 + 2n_2 + 3n_3 + \dots + xn_x)/N$ .

tion potential for catecholamines). When the detector was moved several microns away from the cell, the signals became smaller and slower. Stimulating with longer depolarizations generally led to an increase in the number and frequency of unitary events, not to an increase in their individual size (Fig. 1b). These observations suggest that the signals represent packages of oxidizable substance being secreted from the cell, in agreement with a previous report on unclamped cells<sup>5</sup>.

Another way to monitor secretion from single cells is to record the membrane capacitance<sup>8,11</sup>. This electrical parameter is proportional to cell surface area and increases when vesicles fuse with the plasma membrane during exocytosis. When a cell was stimulated repetitively (Fig. 2), the time-averaged signal of the carbon-fibre electrode closely resembled the derivative of the capacitance trace, thus confirming that both quantities reflect rate of transmitter release. In another cell (data not shown), short depolarizing pulses each elicited an average of 1.05 unitary events and a 13-fF increment in capacitance. Assuming that each event is due to a single vesicle and that each vesicle contributes 2.5 fF (as suggested from previous measurements<sup>8</sup> and from morphometry), we conclude that the carbon-fibre electrode detected about 15–25% of the quanta released. This compares well with the fraction of the cell surface area in closest apposition to the detector surface (see Fig. 1 legend).

Amperometric currents from secreting chromaffin cells arise almost exclusively from oxidation of catecholamine molecules<sup>6</sup>, and each molecule contributes two electronic charges<sup>12</sup>. Thus, one can estimate the number of catecholamine molecules per transient from the total charge of the unitary signal. Figure 1c shows a histogram of the integrals of the current transients from three cells. From its mean the number of molecules detected can be calculated as 2.4–3.2 million (see Fig. 1 legend), agreeing with previous estimates ( $3 \times 10^6$  molecules) for single bovine chromaffin granules<sup>13</sup>.

For synapses the number of vesicles released per stimulus follows binomial or Poisson statistics<sup>1</sup>. As shown in Table 1, such statistics also apply to secretion from chromaffin cells. Although the unitary events are not as uniform as miniature synaptic currents, they are generally well separated in time (for submaximal stimuli), making it possible to count them directly (something not possible for postsynaptic signals except at very low temperatures and low calcium<sup>14</sup>).

\* To whom correspondence should be addressed.



Unlike the neuromuscular junction<sup>1</sup>, the squid giant synapse<sup>2,3</sup> or neurons<sup>4</sup>, for which synaptic events occur about 1 ms after stimulation, the latency in chromaffin cells is quite long at  $51 \pm 7.3$  ms (see Fig. 1d for an example of a latency histogram). Use of the nystatin method<sup>15</sup> to minimize perturbations of the cytoplasmic constituents did not reduce the latency, ruling out that 'washout' of intracellular mediators artificially prolonged the response time.

When examining specifically single events with fast rise time (events which should report the time course of release most faithfully), we observe something surprising: most of the signals have a small 'foot' or 'pedestal' preceding an abrupt upstroke (see Figs 3 and 1a for examples). One possible explanation could be the near-simultaneous release of two vesicles. At least

two findings rule out such a hypothesis, however, unless a very strong, time-dependent correlation between the two release events is postulated (see legend to Fig. 3). First, the mean time between the 'foot' event and the main event is much shorter than the time interval expected for two independent events on the basis of the latency distribution. Second, the mean amplitude of the foot event is much smaller than the overall mean. The latter finding in particular makes the hypothesis of superposition very unlikely. One would have to postulate that small events (expected to occur far from the recording carbon electrode) routinely precede large events (which probably occur close to the electrode). Although such a possibility cannot be totally excluded yet, we favour an interpretation in which pedestal and upstroke result from the same fusion event. If so, a likely

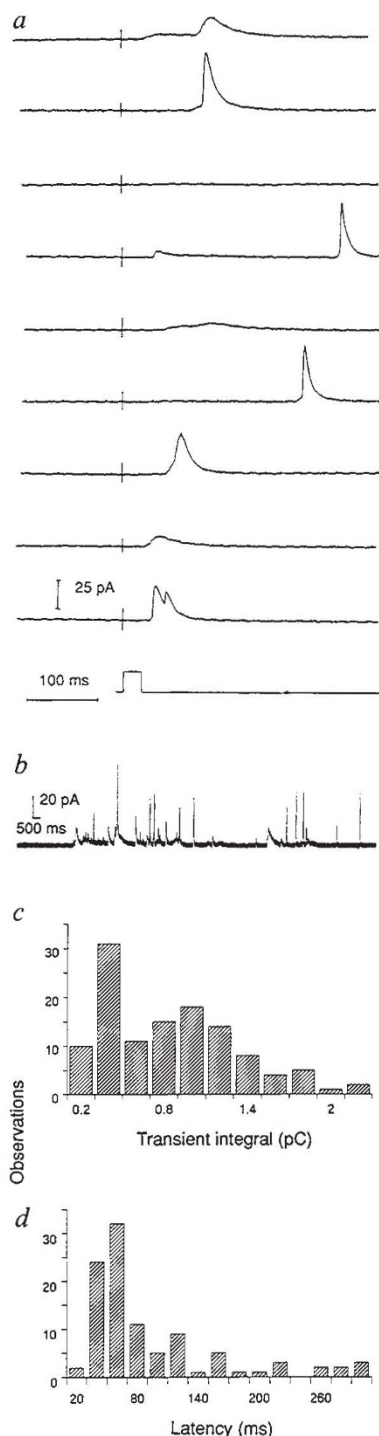


FIG. 1 Electrochemical approach detects secretion from single vesicles. *a*, Examples of signals recorded by the amperometric constant-voltage method. A cell (diameter  $\sim 15 \mu\text{m}$ ) in the whole-cell patch-clamp mode was held at  $-60$  mV and repetitively depolarized to  $+10$  mV for 25 ms to activate  $\text{Ca}^{2+}$  channels. The tip of a carbon-fibre electrode (diameter  $8 \mu\text{m}$ ), located  $<1 \mu\text{m}$  from the cell (with the voltage held constant at  $800$  mV), recorded the evoked secretory signals. If the fibre tip detects molecules released from the cell surface that lies within the projection of a  $12\text{-}\mu\text{m}$  disc, we estimate that about 15% of all events should be detected. The voltage protocol is shown in the bottom trace, and representative amperometric current signals are shown above, aligned in time relative to the stimulating pulse. The signals vary in amplitude and duration, and occasionally there are 'failures' (sweeps without a response). *b*, Response to steady-state depolarization to  $0$  mV after the recording of part *a* (note difference in time scales). *c*, Histogram of integrals of current transients in picocoulombs (pC). For 3 cells, all current transients having a fast rise time ( $<3$  ms) were selected, because these signals presumably arise from vesicles opening closest to the detector. Time integrals of 84 current transients were plotted as a histogram. One extra large event is not included because it is off the scale (at  $3.4$  pC). In some other experiments, particularly after prolonged stimulation, such extra large events were more numerous. They may represent multigranular exocytosis<sup>22</sup>. The charge per transient (mean  $\pm$  s.d.) is  $0.76 \pm 0.55$  pC, equivalent to  $2.36 (\pm 1.71) \times 10^6$  molecules of catecholamine. The histogram includes small events with short rise times which were probably due to vesicles opening close to the detector, but near its rim (where some molecules may diffuse away and escape detection). Excluding such small and fast 'rim' events by setting an amplitude threshold ( $20$  pA), gives a mean charge of  $1.00 \pm 0.53$  pC or  $3.15 (\pm 2.61) \times 10^6$  molecules. *d*, Histogram of latency times (the time between beginning of the depolarizing step and the onset of the current transient). Release probability is high during the first  $100$  ms, and then drops to a lower but maintained value, which, at a compressed timescale, appears as another slow component with a decay time in the range of seconds. Such slow components were present in different cells to various degrees (comprising 23–53% of all events). In 4 cells the mean latency of the fast component was  $51 \pm 7.3$  ms (mean  $\pm$  s.e.m.).

**METHODS.** Bovine chromaffin cells were prepared as previously described<sup>23</sup> and kept for 1–5 days in short-term culture. Voltage-clamp control of membrane potential was achieved using the whole-cell patch-clamp method<sup>24</sup> or else the nystatin method<sup>15</sup>. Extracellular solution in mM:  $120$  NaCl;  $2$   $\text{CaCl}_2$ ;  $2$   $\text{MgCl}_2$ ;  $10$  Na-HEPES;  $50$  glucose; pH  $7.2$ . Pipette solution:  $145$  Cs-glutamate;  $8$  NaCl;  $1$   $\text{MgCl}_2$ ;  $2$  Mg-ATP;  $0.3$  GTP;  $10$  Na-HEPES; pH  $7.2$ ;  $0.1$  Fura-2. Amperometric constant-voltage measurements were done as described<sup>5,6</sup>, with some modifications in the method of preparation of the electrodes<sup>25</sup>. A  $4\text{-}$  to  $5\text{-cm}$  length of  $8\text{-}\mu\text{m}$  diameter carbon fibre was cannulated into  $0.28$  mm inner diameter polyethylene tubing, the middle of which was subsequently heated over a hot soldering iron tip. When melted, the tubing was pulled gently apart  $1\text{--}2$  cm, resulting in a narrowed region where the melted plastic formed an electrically tight seal with the carbon fibre. The narrowed region was cut by scissors, resulting in two electrodes with carbon exposed only at the very tips. Each such assembly was glued in a glass capillary tube, which was then back-filled with  $3$  M KCl solution. Electrical connection to an EPC-7 patch-clamp headstage was established through an Ag/AgCl wire inserted into the KCl solution. During experiments, the voltage of the electrode was set to  $800$  mV and the tip of the carbon-fibre electrode pushed gently against the cell. The oxidation currents were filtered in two stages at  $10$  kHz and  $3$  kHz, digitized and stored on a video cassette recorder. Experiments were done at room temperature ( $22\text{--}30^\circ\text{C}$ ).



FIG. 2 Correlation between the amperometric signal and the rate of capacitance change. A cell was held at  $-60$  mV and repetitively depolarized to  $0$  mV for about  $8$  s at a time (see lowest trace for voltage protocol). Capacitance (second trace from bottom) increased during depolarizations, and the amperometric signal (third trace from bottom) displayed peaks. The time derivative of the capacitance signal, which, like the amperometric signal, should be proportional to secretion rate, is displayed in the top trace (in femtofarads per second) for comparison with the latter.

METHODS. Whole-cell membrane current was recorded with a computer-controlled patch-clamp amplifier (EPC-9), which provides a routine for automatic compensation of cell capacitance. This routine can be repeated (capacitive tracking mode), with an analogue output signal proportional to capacitance. The latter signal was sampled together with the amperometric signal and with membrane voltage, averaged over  $0.5$ -s intervals, and stored on a computer for later analysis and plotting. The time derivative of the capacitance signal was calculated numerically, averaging over four neighbouring datapoints.

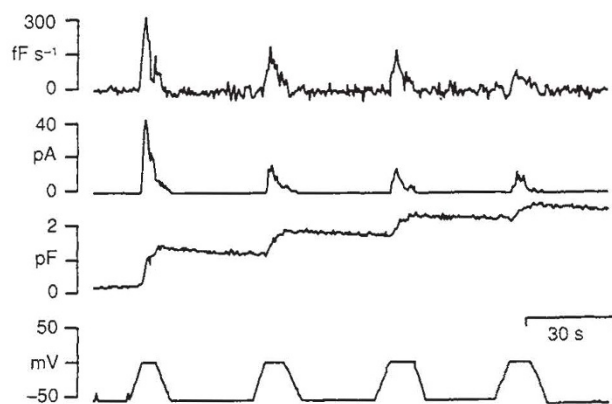
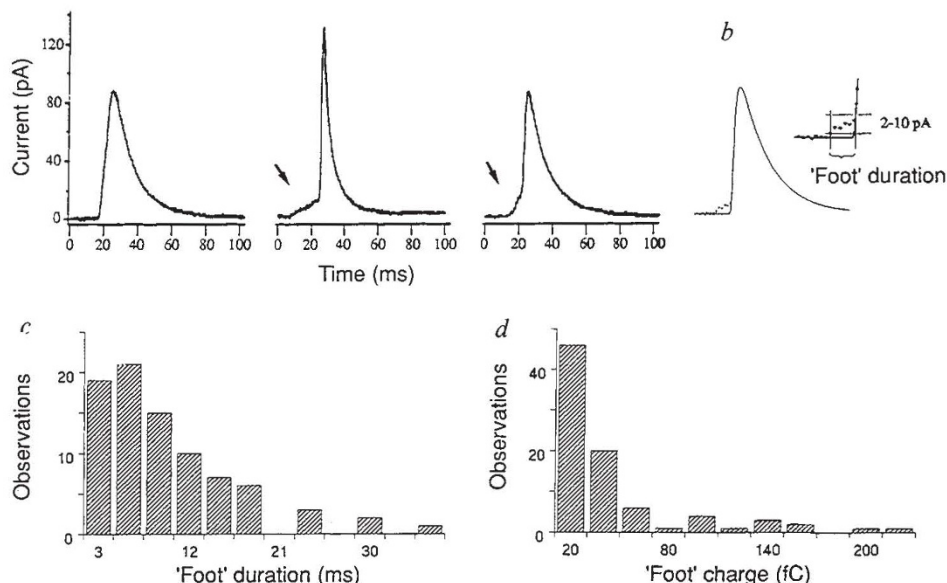


FIG. 3 Rising phase of amperometric current transients cannot be explained by instantaneous release of secretory vesicle contents. *a*, Single amperometric current transients at high resolution. Note that the fast rising phase in two out of the three examples is preceded by a small pedestal or 'foot' (arrows). Such 'foot' signals precede most of the transients with a fast rise time. The 'foot' signals were typically much smaller than the average signal. In one cell, 139 transients were counted, 51 of which were large ( $>20$  pA). Of these large signals, 41 had a small ( $<20$  pA) 'foot' starting within  $20$  ms of the main event, and in only two cases were there two large events within  $20$  ms of each other. If the 'foot' events followed the same amplitude distribution as the main events, one would expect about 12 to be large. *b*, Simulation of transient. The trace shown is the analytical solution for one-dimensional diffusion for the instantaneous release of  $4.5$  million molecules from the surface of an infinite reflecting plane, separated by distance  $x$  from a parallel infinite absorbing plane (as determined using the standard method of image planes<sup>26,27</sup>). The flux  $J$  into the absorbing plane is given by



$$J = \sum_i (-1)^i \frac{M(x-2ix)}{2t\sqrt{\pi Dt}} \exp\left(-\frac{(x-2ix)^2}{4Dt}\right)$$

with  $M = 4.5 \times 10^6$ ,  $D = 3 \times 10^{-7}$  cm<sup>2</sup> s<sup>-1</sup>,  $x = 10^{-4}$  cm, and the sum extended from  $i = -7$  to  $i = 8$ . Drawn superimposed over part of the analytical solution is a typical 'foot'. Inset, 'Foot' region shown at expanded scale, with markers denoting the parameters measured in our analysis procedure. We defined the beginning of the 'foot' as the time when the signal exceeded the peak-to-peak noise of a  $5$ -ms time segment (typically  $1$ – $2$  pA) and the

end of the 'foot' as the time point when the signal exceeded a typical 'foot' amplitude ( $\approx 10$  pA). When these criteria were applied to the analytical signal, a 'foot' duration of  $0.7$  ms was obtained. Thus, the inaccuracy of our 'foot' duration' should be that order of magnitude. *c*, Histogram of duration of 'foot' signals. Data from three cells are pooled, where  $84$  large ( $>20$  pA) and fast (rise time  $< 3$  ms) signals were counted.  $75$  of those were preceded by a discernible 'foot'. The number of occurrences is plotted against the duration of the 'foot', as defined in *a*. The mean of 'foot' durations was  $8.26$  ms. Based on the latency distribution one would expect the mean interval to be  $20$ – $30$  ms, if the 'foot' and the main event were independent. *d*, Histogram of 'foot' charges. The same 'foot' signals as those of *c* were integrated to calculate the charge involved. Mean charge:  $34$  fC or  $1.05 \times 10^5$  molecules. The mean amplitude of the 'foot' signal was  $7.17 \pm 5.28$  pA (mean  $\pm$  s.d.).

explanation could be that the pedestal arises from the slow leakage of catecholamines through a so-called 'fusion pore' which is postulated to occur as an early step in exocytosis<sup>16</sup>. Fusion pores are believed to be gap-junction-like structures<sup>17</sup> which form as a nucleus for fusion, and then, after some delay, dilate to complete the fusion process.

The observation of the long latency for exocytosis in chromaffin cells has profound implications for the underlying molecular mechanisms. At the neuromuscular junction and at the squid giant synapse fast kinetics of transmitter release have been explained either by a direct effect of voltage on the release process<sup>18</sup> or alternatively by the fast buildup and collapse of microdomains of highly elevated calcium concentration<sup>19,20</sup>. Such domains, in which the internal  $\text{Ca}^{2+}$  concentration can rise above  $100$   $\mu\text{M}$ , are expected to occur in the immediate vicinity of open calcium channels. Neither of these mechanisms

seems to apply to the 'slow' secretion from neuroendocrine cells. The majority of secretory events occurs  $5$ – $100$  ms after the end of a voltage pulse stimulus. Thus, membrane potential has been long restored to resting values, and  $\text{Ca}^{2+}$ -microdomains have collapsed (this occurs within microseconds after closing of channels) by the time the vesicles fuse. A theory explaining exocytosis in chromaffin cells must therefore assume either that calcium or membrane depolarization triggers a cascade of events that manifests itself only later, or else that exocytosis occurs predominantly at intermediate calcium concentration ( $5$ – $30$   $\mu\text{M}$ ), which prevail in a submembraneous shell for times of about  $100$  ms<sup>21</sup>.

**Note added in proof:** Since the submission of this paper, Wightman *et al.*<sup>28</sup> have published a paper that provides further evidence that the individual amperometric signals are due to single vesicle fusion events. □



Received 2 October; accepted 5 December 1991.

- Del Castillo, J. & Katz, B. *J. Physiol., Lond.* **124**, 560-573 (1954).
- Linas, R., Steinberg, I. Z. & Walton, K. *Biophys. J.* **33**, 323-352 (1981).
- Augustine, G. J., Charlton, M. P. & Smith, S. J. *J. Physiol., Lond.* **367**, 163-181 (1985).
- Edwards, F. A., Konnerth, A. & Sakmann, B. *J. Physiol., Lond.* **430**, 213-249 (1990).
- Leszczynski, D. J. et al. *J. Biol. Chem.* **265**, 14736-14737 (1990).
- Leszczynski, D. J. et al. *J. Neurochem.* **56**, 1855-1863 (1991).
- Fenwick, E. M., Marty, A. & Neher, E. *J. Physiol., Lond.* **331**, 599-635 (1982).
- Neher, E. & Marty, A. *Proc. natn. Acad. Sci. U.S.A.* **79**, 6712-6716 (1982).
- Duchen, M. R., Millar, J. & Biscoe, T. J. *J. Physiol., Lond.* **426**, 5 (1991).
- Marsden, C. A. et al. *Neuroscience* **25**, 389-400 (1988).
- Lindau, M. & Neher, E. *Pflügers Arch.* **411**, 137-146 (1988).
- Baur, J. E., Kristensen, E. W., May, L. J., Wiedemann, D. J. & Wightman, R. W. *Analyt. Chem.* **60**, 1268-1272 (1988).
- Phillips, J. H. *Neuroscience* **7**, 1595-1609 (1982).
- Katz, B. & Miledi, R. *J. Physiol., Lond.* **181**, 656-670 (1965).
- Horn, R. & Marty, A. *J. gen. Physiol.* **92**, 145-159 (1988).
- Almers, W. A. *Rev. Physiol.* **52**, 607-624 (1990).
- Thomas, L. et al. *Science* **242**, 1050-1053 (1988).
- Parnas, H., Dudel, J. & Parnas, I. *Pflügers Arch.* **406**, 121-130 (1986).
- Simon, S. M. & Linas, R. *Biophys. J.* **48**, 485-498 (1985).
- Fogelson, A. L. & Zucker, R. S. *Biophys. J.* **48**, 1003-1017 (1985).
- Sala, F. & Hernandez-Cruz, A. *Biophys. J.* **57**, 313-324 (1990).
- Alvarez De Toledo, G. & Fernandez, J. M. *J. gen. Physiol.* **95**, 397-409 (1990).
- Marty, A. & Neher, E. *J. Physiol., Lond.* **367**, 117-141 (1985).
- Hamill, O. P., Marty, A., Neher, E., Sakmann, B. & Sigworth, F. J. *Pflügers Arch.* **391**, 85-100 (1981).
- Armstrong-James, M. & Millar, J. *J. Neurosci. Meth.* **1**, 279-287 (1979).
- Crank, J. *The Mathematics of Diffusion* 2nd edn (Oxford University Press, Oxford, 1975).
- Jackson, J. D. *Classical Electrodynamics* 2nd edn (Wiley, New York, 1975).
- Wightman, R. M. et al. *Proc. natn. Acad. Sci. U.S.A.* **88**, 10754-10758 (1991).

ACKNOWLEDGEMENTS. We thank F. Sigworth for providing the analytical approach to solving the one-dimensional diffusion equation, M. Pilot and M. Papke for technical assistance and J. Millar, M. Duchen and R. M. Wightman for advice on carbon-fibre electrodes and for providing information on unpublished work. This work was supported by the Deutsche Forschungsgemeinschaft.

## Prevention of experimental autoimmune encephalomyelitis by antibodies against $\alpha 4 \beta 1$ integrin

Ted A. Yednock, Catherine Cannon,  
Lawrence C. Fritz, Francisco Sanchez-Madrid\*,  
Lawrence Steinman† & Nathan Karin†

Athena Neurosciences, South San Francisco, California, USA

\* Universidad Autonoma de Madrid, Madrid, Spain

† Stanford University, Stanford, California, USA

**EXPERIMENTAL** autoimmune encephalomyelitis (EAE) is an inflammatory condition of the central nervous system with similarities to multiple sclerosis<sup>1,2</sup>. In both diseases, circulating leukocytes penetrate the blood-brain barrier and damage myelin, resulting in impaired nerve conduction and paralysis<sup>3-5</sup>. We sought to identify the adhesion receptors that mediate the attachment of circulating leukocytes to inflamed brain endothelium in EAE, because this interaction is the first step in leukocyte entry into the central nervous system. Using an *in vitro* adhesion assay on tissue sections, we found that lymphocytes and monocytes bound selectively to inflamed EAE brain vessels. Binding was inhibited by antibodies against the integrin molecule  $\alpha 4 \beta 1$ , but not by antibodies against numerous other adhesion receptors. When tested *in vivo*, anti- $\alpha 4$  integrin effectively prevented the accumulation of leukocytes in the central nervous system and the development of EAE. Thus, therapies designed to interfere with  $\alpha 4 \beta 1$  integrin may be useful in treating inflammatory diseases of the central nervous system, such as multiple sclerosis.

EAE was induced in Lewis rats by a single intraperitoneal injection of a CD4-positive T-cell clone specific for myelin basic protein<sup>6</sup>. These cells have been shown to localize in the central nervous system (CNS) within 4-12 h, where they initiate inflammation<sup>7</sup>. Endogenous monocytes and lymphocytes infiltrate inflamed vessels in the brain stem and spinal cord, leading to paralysis of the tail and hind limbs on days 4 and 5. The degree of leukocyte infiltration at the time of paralysis is shown in Fig. 1. Inflamed vessels were never found in brains of control animals.

TABLE 1 Antibodies against  $\alpha 4 \beta 1$  integrin inhibit U937, monocyte and lymphocyte binding to inflamed vessels in EAE brain sections

(a) Treatment of U937 cells		Relative binding to EAE vessels (% of control)
Anti- $\beta 1$ integrin	AIIB2	8 ± 3
Anti- $\alpha 3$ integrin	A043	111 ± 5
Anti- $\alpha 4$ integrin	HP2/1 (inhibits FN and VCAM-1-binding)	3 ± 1
Anti- $\alpha 4$ integrin	P4G9 (selectively inhibits FN binding)	151 ± 7
Anti- $\alpha 4$ integrin	HP1/7 (selectively inhibits FN binding)	338 ± 41
Anti- $\alpha 5$ integrin	P1D6	104 ± 6
Anti- $\alpha 6$ integrin	GoH3	88 ± 11
Anti- $\alpha 4$ , and - $\alpha 5$	P4G9 and P1D6 (combined)	138 ± 8
Anti- $\alpha 3$ , - $\alpha 4$ , and - $\alpha 6$	A043, P1D6, and GoH3 (combined)	112 ± 3
Anti-CD44	Hermes-3	107 ± 4
Anti-L-selectin	TQ-1	96 ± 4
Anti- $\beta 2$ integrin	P4H9	77 ± 1
Anti- $\beta 2$ integrin	TS1/18	98 ± 5
Anti- $\beta 2$ integrin	P4H9 (tested at 25 °C)	100 ± 10
Anti- $\beta 2$ integrin	TS1/18 (tested at 25 °C)	114 ± 2
Anti- $\alpha 4$ integrin	HP2/1 (tested at 25 °C)	5 ± 1
Anti-LFA-1	10T16	123 ± 2
Anti-Mac-1	LM2/1	107 ± 3
(b) Treatment of freshly isolated lymphocytes or monocytes		
Antibody specificity	Clone	Cell type
Anti- $\beta 1$ integrin	AIIB2	human lymphocytes
Anti- $\alpha 4$ integrin	HP2/1	human lymphocytes
Anti- $\alpha 4$ integrin	HP2/1	human monocytes
Anti- $\alpha 4$ integrin	HP2/1	rat lymphocytes
Anti- $\alpha 4$ integrin	R1-2	mouse lymphocytes
Anti-CD2	OX-34	rat lymphocytes
Anti-L-selectin	MEL-14	mouse lymphocytes
Peyer's patch homing receptor	1B.2.6	rat lymphocytes
Anti-LFA-1	OX-52	rat lymphocytes
Anti-CD45	OX-1	rat lymphocytes
Anti-Thy 1.1	OX-7	rat lymphocytes
Anti-CD4	OX-35	rat lymphocytes
Anti-monocyte/T cell surface	OX-44	rat lymphocytes
		Relative binding to EAE vessels (% of control)
		7 ± 2
		0 ± 0
		1 ± 1
		18 ± 7
		43 ± 2
		100 ± 10
		92 ± 4
		117 ± 12
		87 ± 1
		90 ± 3
		087 ± 3
		107 ± 5
		102 ± 8

a. Analysis of antibodies against cell adhesion molecules revealed that only reagents against  $\alpha 4 \beta 1$  integrin significantly affected binding of U937 cells to EAE vessels. Expression of  $\beta 1$  integrins by U937 given as mean fluorescence channel number determined by FACS analysis: no primary antibody, 4;  $\alpha 1$  (TS2/7), 3;  $\alpha 2$  (G19), 5;  $\alpha 3$  (A043), 25;  $\alpha 4$  (HP2/1), 189;  $\alpha 5$  (P1D6), 62;  $\alpha 6$  (GoH3), 40.

b. The attachment of human peripheral blood lymphocytes and monocytes to EAE vessels was also inhibited by the anti-human  $\alpha 4$  integrin antibody, HP2/1. This antibody crossreacts with rat lymphocytes and inhibits their binding to inflamed brain venules (although threefold higher concentrations of HP2/1 were required for maximal inhibition, and inhibition was not as complete as with human lymphocytes). An antibody against mouse  $\alpha 4$  integrin (R1-2) was less effective but substantially inhibited the attachment of mouse lymphocytes to EAE vessels. Cells were treated with saturating concentrations (determined by FACS analysis) of the indicated antibodies on ice for 30 min before the *in vitro* section assay, as described in Fig. 2—which was usually done in the continued presence of the antibody. In several experiments, the cells were washed out of HP2/1 (anti- $\alpha 4$ ) and AIIB2 (anti- $\beta 1$ ) with no diminution of their inhibitory effect. Binding was quantified using an internal standard population of cells as previously described<sup>30</sup>. Numbers indicated in the table represent the percentage of binding relative to the control with no antibody ( $\pm$ s.e.m.), and is based on counting cells bound to at least 10 vessels in each of 3-6 independent sections. Antibody sources: HP2/1, HP1/7 have been described<sup>14</sup>; AIIB2, gift from C. H. Damsky, University of California, San Francisco; Hermes-3, gift from E. C. Butcher, Stanford University; 1B.2.6, gift from Y. H. Chin, University of Miami; A043, P4G9, P1D6 and P4H9, Telios Pharmaceuticals, San Diego; Gi9, GoH3 and 10T16, AMAC, Westbrook, Maine; OX-1, OX-7, OX-34, OX-35, OX-44 and OX-52, Bioproducts for Science, Indianapolis; TS2/7, T Cell Sciences, Cambridge, Massachusetts; TQ-1, Coulter Immunology, Hialeah, Florida; TS1/18, ATCC number HB 203; LM2/1, ATCC number HB 204; R1-2, ATCC number HB 227; and MEL-14, ATCC number HB 132.

Sections of day 5 EAE brain were tested for their ability to support leukocyte attachment in a modified Stamper-Woodruff *in vitro* binding assay<sup>8</sup>. Human monocytic cells of line U937 bound selectively to inflamed venules exposed in 10- $\mu$ m sections of EAE brain (Fig. 2), and occasionally to small arterioles (not shown), but never to vessels in sections of noninflamed brain. Binding was restricted to the lumen of the vessels, consistent with an endothelial interaction (Fig. 2). Comparable binding